Electrochemical reactivity of In-Pb solid solution as a negative electrode for rechargeable Mg-ion batteries

Lucie Blondeau, Suzy Surblé, Eddy Foy, Hicham Khodja, Magali Gauthier

Electrochemical reactivity of In-Pb solid solution as a negative electrode for rechargeable Mg-ion batteries

Lucie Blondeau[a], Suzy Surblé[a], Eddy Foy[b], Hicham Khodja[a], Magali Gauthier[a,*]

[a]*Université Paris-Saclay, CEA, CNRS, NIMBE, LEEL, 91191, Gif-sur-Yvette, France*

[b]*Université Paris-Saclay, CEA, CNRS, NIMBE, LAPA-IRAMAT, 91191, Gif-sur-Yvette, France*

[*]Corresponding author. E-mail address: magali.gauthier@cea.fr (M. Gauthier).

Abstract

A composite In-Pb:carbon was successfully synthetized by a two-step mechanochemical synthesis in order to obtain an adequate particles size and structure to investigate the electrochemical reactivity of the In-Pb solid solution towards Mg. A potential synergetic coupling of electroactive elements In and Pb was examined using electrochemical and *ex situ* X-ray diffraction analyses. The potential profile of the solid solution indicates the formation of Mg_2Pb and MgIn. However, the diffraction study suggests a peculiar electrochemically-driven amorphization of MgIn during the magnesiation, in strong contrast to MgIn crystallization in In-based and InBi-based electrodes reported in the literature. Combining In and Pb favors the amorphization of MgIn and a high first magnesiation capacity of about 550 mAh g^{-1}, but is thereafter detrimental to the material's reversibility. These results emphasize the possible influence of electrochemically-driven amorphization and crystallization processes on electrochemical performance of battery materials.

Keywords: Magnesium battery; Negative electrode; Alloy; Amorphization

1. Introduction

The exchange of multivalent cations (Mg^{2+}, Ca^{2+}, Al^{3+}) in batteries is a new promising approach with a strong enthusiasm in the scientific community in the last 10–15 years [1–5]. The best example is the development of magnesium metal (Mg) batteries that can exchange two electrons per metal (Mg) compared to only one electron in the case of lithium and sodium. Magnesium appears as a great alternative to lithium due notably to its high volumetric capacity (3833 mAh cm^{-3}) [5], low cost, abundance on Earth and largely smaller reactivity and better safety compared to lithium [2,5]. However, common electrolytes strongly interact with magnesium metal to form a barrier on its surface [3,5], inhibiting any exchange of Mg^{2+} ions between the two electrodes. Only organometallic electrolytes complexes in ethereal-based solvents can be used with magnesium metal [3,5,6], but their narrow potential window and high volatility limit the feasibility of practical Mg batteries.

Unlike pure magnesium metal electrodes, insertion/alloying negative electrodes are apparently not suffering from the formation of a blocking layer to Mg^{2+} ions in conventional electrolytes [7,8], as demonstrated for example with the reversible cycling of bismuth, tin or Bi-Sb alloys electrodes in a $Mg(N(SO_2CF_3)_2)_2$/acetonitrile solution [7–9]. Several *p*-block elements (Bi [7,8,10], In [11], Sn [12], Sb [7] and Pb [13]) have been investigated as a sole element in Mg-based batteries. The best candidate is Bi, which has been studied for example in the form of nanotubes by Shao et al. [8], and can deliver a capacity of 350 mAh g^{-1} for the first cycle with remarkable capacity retention of 300 mAh g^{-1} after 200 cycles and high rates performance. Combining different *p*-block elements appears also as a powerful method to get a synergetic effect, as already shown in the case of SnSb [9] or Bi_xSb_{1-x} [14]. Parent et al. [9] demonstrated that after electrochemical alloying/dealloying with Mg, SnSb particles are transformed into a network of Sn and Sb sub-particles, where Sn is the electroactive component. While Sb is poorly

active towards Mg, it promotes the electrochemical performance of Sn with the formation of an interface that stabilizes Sn into its cubic phase. Recently, we also demonstrated a beneficial coupling of In and Sb in the InSb alloy, where Sb magnesiation/demagnesiation was shown for the first time to be partially reversible [15].

Here we prospect for a synergetic combination between In and Pb in an In-Pb solid solution using carbon (In-Pb:C) to reduce particles size. The goal was to use both In and Pb advantages while minimizing their limitations. The benefits of Pb are its low polarization, high theoretical capacity (517 mAh g^{-1}) and its inexpensive character [13], while the main issue is its toxicity [13]. Concerning In, it presents a good reversibility and the lowest alloying potential among *p*-block elements [11], but suffers from kinetics limitations at high rates [11] and scarce resources. The reaction of an In-Pb solid solution with Mg is fundamentally investigated with electrochemical and X-Ray Diffraction measurements. This study mainly highlights how the coupling of In and Pb affects the reaction mechanisms and the structure of the products formed upon reaction with Mg.

2. Experimental

In-Pb and In-Pb:C composite powders were synthesized by high energy mechanochemical synthesis. Indium (Alfa Aesar, -325 mesh, 99.99%) and lead (Alfa Aesar, -200 mesh, 99.9%) powders were used as starting materials in stoichiometric amounts. 30 wt% of carbon (Carbon black Super P, Timcal) was added in the case of the In-Pb:C powders (P1 and P2 samples, see Fig. 1d for details). As a comparison, a In:C powder with 30 wt% carbon was prepared. Powders were placed in a stainless steel vials with 3 stainless-steel balls with a ball-to-powder ratio of 1:70. Ball milling was performed under argon in a Fritsch Pulverisette for 5 h for each step. The milling yield (corresponding to the ratio of powder masses after and before milling) was higher

than 95%, denoting limited welding between the balls or the vial with the powder.

The structure of the synthesized powder was determined by X-ray diffraction (XRD) with a RU-200B rotating anode X-ray generator using Mo $K\alpha_{1,2}$ radiation (λ=0.7093Å) in transmission mode. Spherical diffraction patterns were acquired using a photo-sensitive plate that was digitized using a scanner. The software FIT2D [16] was used to integrate the diffraction patterns. The morphology and composition of the In-Pb and In-Pb:C powders were studied by Scanning Electron Microscopy coupled with energy X-ray dispersive spectroscopy (EDS) using a FESEM JEOL JSM-7001F or a SEM-FEG Carl Zeiss Ultra 55. The Saclay nuclear microprobe was also used to determine In and Pb contents using Particle-Induced X-ray Emission (PIXE) with a proton microbeam of 3×3 μm^2 at 2595 keV.

Composite electrodes were prepared by mixing In-Pb or In-Pb:C powders, poly(vinylidene fluoride) (PVDF, Solef, Solvay) and Super P carbon black (Timcal) in a 80/10/10 mass ratio with N-methyl-2-pyrrolidone (NMP, 99%, Acros Organics) and casted onto a copper foil (99.8%, Alfa Aesar). Electrodes were dried at room temperature for 24 h and then at 120 °C under vacuum for 24 h. Swagelok-type cells were assembled in an argon-filled glovebox. They comprise a disc of composite electrode, a Mg foil (99.95%, Gallium Source LLC) and 2 Whatman GF/A borosilicate glass-fiber separators soaked with electrolyte. The electrolyte consists of a ~ 0.35 mol L^{-1} solution of a complex based on a 1:1 molar ratio of ethylmagnesium chloride (EtMgCl, 2.0 M in tetrahydrofuran, Sigma Aldrich) and diethylaluminum chloride (Et_2AlCl, 97%, Sigma Aldrich) in tetrahydrofuran (THF, 99.9%, Carlo Erba), stirred for 20 h in the glovebox before use. Galvanostatic cycling was performed at C/100 or C/50 rates between 0.005 V_{Mg} and 0.8 V_{Mg} (vs Mg^{2+}/Mg) using a VMP recording system (Biologic). C rate is calculated based on full magnesiation of the active material. Galvanostatic Intermittent Titration Technique (GITT) was

also applied with pulse periods of 1 h at C/50 rate followed by rest periods of 2 h. The capacity is expressed per gram of active material, i.e. In-Pb. Each electrochemical test was repeated at least three times to ensure reproducibility.

Ex situ XRD measurements were carried out on cycled samples after disassembling the cells and rinsing the electrodes with THF to remove the electrolyte solution. To avoid any contact with air, the samples were sealed in Kapton tape in the glovebox prior to analysis.

3. Results and discussion

Mechanical alloying is an easy and powerful method to synthetize intermetallic materials, in particular for Li, Na or Mg batteries [17–20]. In this work, we used a mechanochemical synthesis to produce an In-Pb solid solution with initial composition In/Pb of 50/50 at% (denoted as P0). After the milling process, the expected cubic phase for the solid solution of In in Pb is formed [21,22] (space group $Fm\bar{3}m$, a=4.865(3) Å, Fig. S1). The lattice parameter, slightly higher than the value for the $In_{0.5}Pb_{0.5}$ solution (4.843 Å [22]) indicates a composition closer to $In_{0.4}Pb_{0.6}$. The pure In-Pb phase P0 consists of large particles of around 200 µm (Fig. 1c), probably due to the low melting points of In and Pb favoring welding of the particles. Consequently, no electrochemical response was observed on composite electrodes based on these large particles (Fig. S2). To scale down the particles, a second milling step was applied to the In-Pb powder by adding 30 wt% of carbon as a control process agent (Fig. 1a) to limit particles welding and melting [23]. The In-Pb:C composite obtained is referred in the text as the P1 powder. Introducing carbon successfully helps reducing the particles size by a factor of 20 to 40 (Fig. 1d). The P1 In-Pb:C powder is composed of polydispersed agglomerates (10 to 20 µm) made of micrometric sub-particles roughly welded together (Fig. 1d). As a comparison, an In-Pb:C composite with similar particle size (SEM, Fig. S3), referred as P2, was also synthesized in

a one-step milling process by mixing together In, Pb and C elemental powders for 10 h (In:Pb molar ratio 1:1 with 30 wt% of carbon, Fig. 1a).

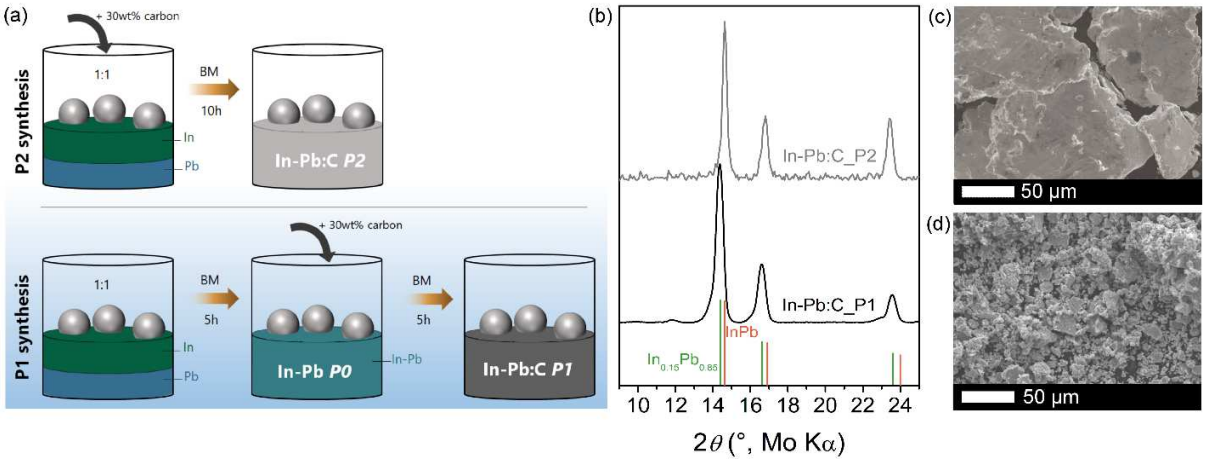

Fig. 1. (a) Schematic showing the experimental protocol for the ball-milling (BM) syntheses of P1 and P2 In-Pb:C powders. (b) XRD patterns of the P1 (black) and P2 (gray) In-Pb:C powders with InPb [22] (red) and $In_{0.15}Pb_{0.85}$ [24] (green) Bragg positions as references. (c, d) Scanning Electron Microscopy (SEM) images of the ball-milled In-Pb P0 and ball-milled composite In-Pb:C P1 powders, respectively.

Both P1 and P2 In-Pb:C composites adopt a cubic phase (Fig. 1b, space group $Fm\bar{3}m$). While the P2 powder closely matches the $In_{0.5}Pb_{0.5}$ solid solution [22] (a= 4.855(1) Å, $In_{0.44}Pb_{0.56}$, Fig. S4), the P1 powder obtained through two milling steps (Fig. 1a) shows an increase of the lattice parameter denoting a lower In content in the powder (a=4.928(6) Å, Fig. S5). Based on the Vegard's law [25], the lattice parameter found for the In-Pb:C P1 composite is close to the composition $In_{0.15}Pb_{0.85}$ [21,24]. P1 apparent sub-stoichiometry in In could denote a loss of In during the two-step milling process. However, unlike XRD data, elemental compositions determined by EDS and PIXE (Table S1 and Fig. S6) evidence an In/Pb molar ratio of 1.0(1) for

P1, showing that the initial stoichiometry 1:1 is maintained. A spread in composition of the powder [25] could explain the discrepancy between XRD and composition, or the presence of pure In, implying a mixture of $In_{0.15}Pb_{0.85}$ and In phases in the powder. Knowing that no crystalline In is observed on the XRD pattern, we infer that the pure In phase could only be amorphous. While P1 and P2 samples share a similar In/Pb molar ratio (1.0(1) for P1 and 1.1(1) for P2, see SI, Figs. S6 and S7), their crystalline structures differ, from a well-crystalline $In_{0.5}Pb_{0.5}$ phase for the P2 powder to an In-deficient crystalline phase apparently mixed with amorphous In for the P1 powder. Following elemental composition values and to simplify the comparison, we based our calculations for electrochemical measurements on a In/Pb molar ratio of 1 in the P1 and P2 In-Pb:C powders. If considering the mixture [$In_{0.15}Pb_{0.85}$ + 0.7In] instead of $In_{0.5}Pb_{0.5}$ for P1, the error on the capacity calculation is only of 1% (see Supplemental Information (SI)).

Fig. 2(a) compares the first few galvanostatic cycles of In-Pb:C/Mg cells at a C/100 rate for the P1 and P2 samples. The first magnesiation of the P1 sample leads to the reaction of ~2.9 Mg^{2+} with In-Pb in the In-Pb:C composite (Fig. 2a, bottom), close to the theoretical value of 3 based on the formation of Mg_2Pb and MgIn (Reactions (1) and (2)) for an initial In-Pb formula unit (see SI for details):

$$In + Mg^{2+} + 2e^- \rightarrow MgIn \qquad (1)$$

$$In_{0.15}Pb_{0.85} + 1.85Mg^{2+} + 3.7e^- \rightarrow 0.15MgIn + 0.85Mg_2Pb \qquad (2)$$

(1) and (2) combine to give reaction (3) :

$$0.824\mathrm{In} + 1.18\,\mathrm{In_{0.15}Pb_{0.85}} + 3\mathrm{Mg^{2+}} + 6\mathrm{e^-} \rightarrow \mathrm{MgIn} + \mathrm{Mg_2Pb} \quad (3)$$

Peculiarly, the pure crystalline $In_{0.5}Pb_{0.5}$ phase of the P2 powder presents in contrast poor cycling performance (Fig. 2a, top) with ~ 1.75 Mg^{2+} reacting with P2 for the first magnesiation and a sharp capacity decrease on the subsequent cycles. The particular structure and composition of the P1 powder seems to stimulate the reactivity of the In-Pb solid solution. The two-steps ball milling must create particular microstructure or interfaces between carbon, In-Pb and In phases that favor the diffusion of Mg^{2+} in the structure. The creation of defects or vacancies in the In-deficient P1 In-Pb powder could also facilitate Mg paths and reactivity. The properties that promote the reactivity of the P1 powder compared to the P2 powder are currently under investigation. In light of the electrochemical profiles, the results presented from this point only focus on the P1 sample performance and electrochemical behavior.

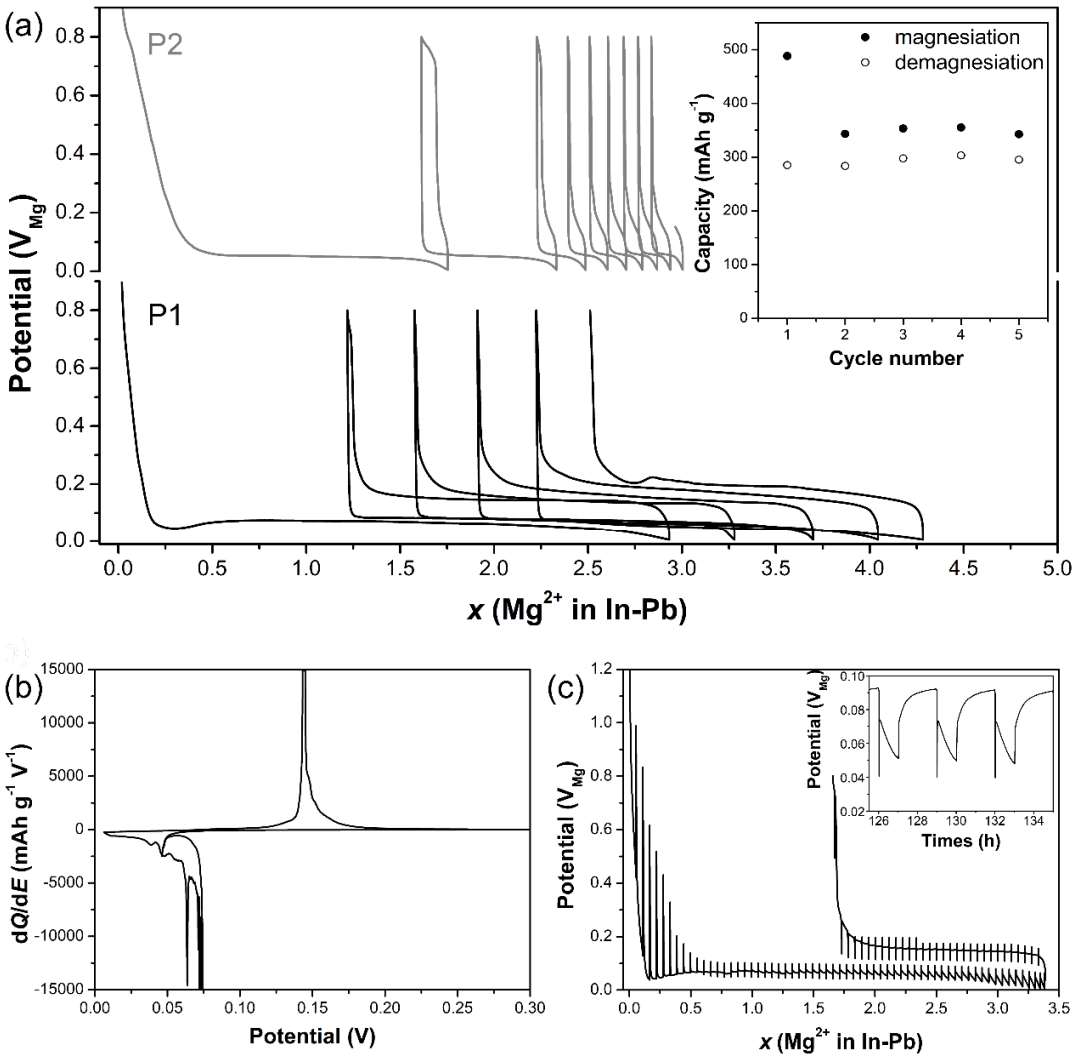

Fig. 2. (a) Magnesiation/demagnesiation curves of In-Pb:C/Mg cells with the P1 and P2 powders cycled at a C/100 rate. The value of *x* is expressed as the number of Mg that reacts with the In-Pb active phase in the In-Pb:C composite. The inset shows the evolution of the magnesiation and demagnesiation capacities along 5 cycles of the P1 sample. (b) Incremental capacity curve corresponding to the first cycle of P1 sample in (a). (c) GITT profile of a P1 powder-based In-Pb:C/Mg cell cycled with pulses of 1 h at C/50 rate followed by open-circuit voltage periods of 2 h. The inset represents the evolution of potential as function of time over three pulses and open-circuit voltage (OCV) periods.

The first magnesiation capacity of the P1 sample is 488 mAh g_{In-Pb}^{-1}, close to the theoretical capacity of 494 mAh g^{-1} for an In/Pb molar ratio of 1 (see SI). A large irreversibility is observed after the first demagnesiation (Fig. 2a), only 58% of the magnesiation capacity is recovered. The voltage polarization is about 70 mV at the first cycle and increases gradually upon further cycling, indicating poor kinetics. Optimization of the particles size should improve the polarization of the material. At the very beginning of the first magnesiation, the potential falls down quickly to ~0.07 V_{Mg} before reaching the alloying plateau (Fig. 2a). As already observed in the literature [7,11–13], this should relate to a nucleation process. The first magnesiation apparently consists of a single plateau ~ 70–80 mV_{Mg}, close to the two-phase reaction potential of In (~60 mV_{Mg} [11]) leading to MgIn. However, the incremental capacity curve (Fig. 2b) corresponding to the first cycle of the In-Pb:C electrode displays two cathodic peaks centered at ~72 and 60 mV_{Mg} that evidences two biphasic processes with the alloying plateaus of Pb (100mV_{Mg} for Pb [13]) and In related to the formation of Mg_2Pb and MgIn respectively. During the demagnesiation, only one broad peak is observed at 0.14 V_{Mg}. This peak may contain both contributions of MgIn and Mg_2Pb as the dealloying plateaus of both phases are quite close [11,13]. A small shoulder can be observed around 0.15 V_{Mg} with a much more rounded profile, often observed when amorphous or poorly crystallized particles are formed [26,27]. An *in situ* nanostructuration of the powder during the electrochemical process could explain the presence of poorly crystallized particles giving rise to the bump at 0.15 V_{Mg}.

To better apprehend thermodynamics and kinetics parameters, a GITT (Galvanostatic Intermittent Titration technique) cycling was applied on the first cycle of an In-Pb:C electrode (Fig. 2c). With this technique, the electrode reaches a steady state after each OCV period, giving access to the thermodynamic potential of the material. The GITT measurement confirms the unique sloppy

plateau at ~100 mV_{Mg} in the GITT, in between the thermodynamic potentials of Mg_2Pb (121 mV_{Mg}) and MgIn (88 mV_{Mg}) (estimated based on their energy of formation (-46.6 and -17 kJ mol^{-1} for Mg_2Pb [28] and MgIn [29,30] respectively)). Looking more in details at few successive periods of pulse (inset in Fig. 2c), one can clearly see that a steady-state potential is not completely reached even after a 2 h OCV period. Combining In and Pb does not improve the kinetic behavior of these two elements.

Ex situ X-ray diffraction was further employed to determine the phases formed upon the reaction of In-Pb:C and Mg. Fig. 3 shows patterns collected on the pristine P1 powder, on electrodes stopped at the end of the magnesiation at a C/100 rate or after the GITT protocol, and finally electrodes stopped at the end of the demagnesiation after 1 and 10 cycles. While the electrochemical measurements (Fig. 2) and the known reactivity of Pb [13] and In [11] with Mg hint at the formation of crystallized Mg_2Pb and MgIn upon magnesiation, our results demonstrate a quite different behavior. After the first alloying reaction at a C/100 rate, an In-Pb phase remains while Mg_2Pb is detected. No pure crystalline In or MgIn (characteristic peaks at 9.3°, 12.6° and 15.6°) is observed. This is opposed to the first magnesiation of In [11] and InBi [18] electrodes where well-crystallized MgIn phases have been detected; but similar to what we already observed in the InSb alloy [15]. It is important to note that the capacity recovered during the cycling of In-Pb cannot be attributed only to the formation of Mg_2Pb alone (see calculations in SI). We thus deduce that, similarly to InSb, the capacity observed implies the formation of MgIn in an amorphous state. This strongly suggests that an electrochemical-driven amorphization of MgIn is taking place during the magnesiation of In-Pb. The amorphization of MgIn during cycling may also be attributed to the presence of carbon in a large quantity during the milling process. Yet, the XRD pattern acquired at the end of the discharge of a In:C (containing 30 wt% C) composite electrode shows clearly the formation of crystalline MgIn (Fig. S8). This confirms that the

particular In-Pb structure is responsible for the amorphization of the MgIn phase.

Differently to InSb [15], no crystalline MgIn is observed even after a complete magnesiation in GITT mode (Fig. 3). In contrast to InSb [15], where the crystallization of MgIn is rate dependent, the amorphization of MgIn seems unavoidable in the In-Pb solid solution. The different crystalline structures of the starting materials can explain the different reactivity of InSb and In-Pb compared to InBi and Bi for example. For InBi and In phases, possessing a tetragonal structure (P4/mmm and I4/mmm), reaction with Mg leads to the formation of crystalline MgIn with the tetragonal P4/mmm structure. The electrochemical formation of MgIn implies thus poor changes in the crystalline structure. On the contrary, the cubic crystalline structure of InSb and In-Pb does not match with tetragonal MgIn, which can account for the amorphization of MgIn. Likewise, during the first electrochemical reaction of Mg^{2+} with In-Pb to form the Mg_2Pb phase, the complete restructuration of the material may also nanostructure the remaining In. This complete rearrangement of In particles could cause the formation of amorphous MgIn upon further reaction of Mg^{2+} at lower potential. The possible presence of amorphous In in the initial powder may also explain the formation of amorphous MgIn.

The presence of a remaining In-Pb phase at the end of magnesiation (Fig. 3) illustrates the poor kinetics of the material. A lack of electrode optimization or a too large particle size, preventing the diffusion of Mg^{2+} in the whole material can also be involved. Surprisingly, at the end of demagnesiation after 1 or 10 cycles, In-Pb cubic phases are solely observed (Fig. 3), with similar diffraction reflections as the pristine powder. While the presence of In and Pb could be expected, the In-Pb intermetallic solid solution is electrochemically reformed, as already observed in the case of InBi [18].

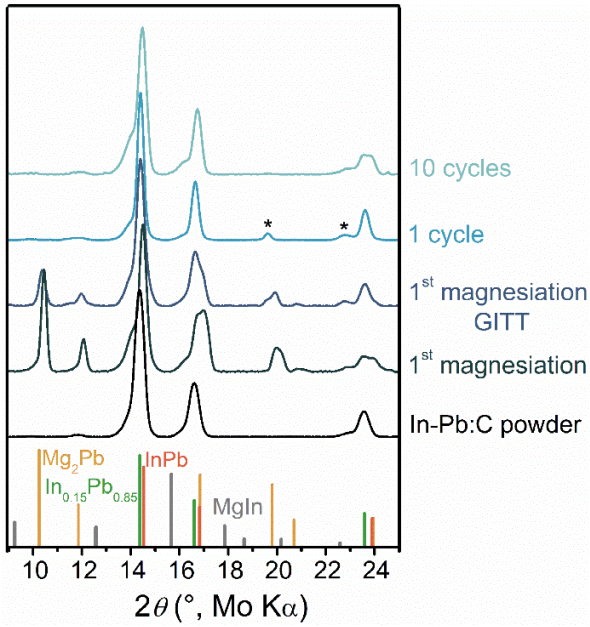

Fig. 3. Ex situ XRD patterns of the composite In-Pb:C powder, electrodes fully magnesiated at a C/100 rate or magnesiated using a Galvanostatic Intermittent Titration Technique (GITT) mode (1 h at C/50 rate followed by 2 h OCV) and electrodes stopped at the end of the demagnesiation after 1 and 10 cycles at C/100 rate. Patterns of InPb ($In_{0.5}Pb_{0.5}$) [22] (red), $In_{0.15}Pb_{0.85}$ [24] (green), Mg_2Pb [31] (yellow) and MgIn [32] (grey) are shown as references. Indexing of reference patterns are gathered in Table S2. * refers to the Cu foil from the current collector.

To evaluate a possible beneficial effect of the combination of In and Pb, the cycling performance of a P1 In-Pb:C electrode was evaluated and is compared below with the literature. Fig. 2(a) (inset) shows the evolution of the magnesiation and demagnesiation capacities upon 5 cycles. A real benefit of the coupling between In and Pb is obtained for the first magnesiation capacity with a value of 488 mAh $g_{\text{active material}}^{-1}$, above the values of ~ 425 and 375 mAh $g_{\text{active material}}^{-1}$ shown in the literature for In [11] and Pb [13] composite electrodes respectively. However, a sharp decrease of the capacity is observed after the first cycle. A reversible capacity of around 300 mAh

g^{-1} is obtained on the following cycles. This is slightly higher than the capacity of a pure Pb composite electrode (~275 mAh g^{-1} [13]) but lower than the capacity observed for In (~420 mAh g^{-1} [11]). Besides, the irreversibility along cycling is similar to the one reported for Pb [13] but higher than the one for In [11]. The poor coulombic efficiency could be explained by a loss of contact between particles due to the large volume changes [10,11,33], the formation of a passivation layer [11,13,33] or some diffusion limitations due to the large particle size [8,13,33]. Above all, the presence of Pb seems to have a detrimental effect on the efficiency of the alloying reaction of Mg with In. A deeper understanding of the reactions underlying the performance of the In-Pb solid solution are needed, notably to determine if the presence of amorphous instead of crystalline MgIn has an impact on the reversibility.

4. Conclusions

Herein, we have evidenced the electrochemical reactivity towards Mg of a composite In-Pb:carbon material successfully synthetized by ball-milling. While the electrochemistry predicts the formation of Mg_2Pb and MgIn, *ex situ* X-ray diffraction experiments on magnesiated electrodes demonstrate the presence of crystalline Mg_2Pb but the absence of crystalline MgIn. While during the magnesiation of In [11] and InBi [18] crystalline MgIn is formed, an electrochemically-driven amorphization of this phase is suggested when In is combined with Pb, as previously observed for InSb [15]. The combination of In with Sb and Pb seems to trigger the amorphization of MgIn. This peculiar phenomenon, involving amorphization of a part of the material when combines with some –but not all– *p*-block elements– should be further studied to rationalize it. This phenomenon echoes the one observed for example in silicon in Li-ion batteries [34] and should guide further research to fully understand the atypical reactivity of alloys in batteries.

Acknowledgments

This work was supported by the Agence Nationale de la Recherche (ANR) of France [grant ANR-16-CE05-0004].

References

[1] D. Aurbach, Z. Lu, A. Schechter, Y. Gofer, H. Gizbar, R. Turgeman, Y. Cohen, M. Moshkovich, E. Levi, Nature 407 (2000) 724–727.
[2] J. Muldoon, C.B. Bucur, T. Gregory, Chem. Rev. 114 (2014) 11683–11720.
[3] R. Mohtadi, F. Mizuno, Beilstein J. Nanotechnol. 5 (2014) 1291–1311.
[4] A. Ponrouch, C. Frontera, F. Bardé, M.R. Palacín, Nat. Mater. 15 (2016) 169–172.
[5] H.D. Yoo, I. Shterenberg, Y. Gofer, G. Gershinsky, N. Pour, D. Aurbach, Energy Environ. Sci. 6 (2013) 2265–2279.
[6] T.D. Gregory, R.J. Hoffman, R.C. Winterton, J. Electrochem. Soc. 137 (1990) 775–780.
[7] T.S. Arthur, N. Singh, M. Matsui, Electrochem. Commun. 16 (2012) 103–106.
[8] Y. Shao, M. Gu, X. Li, Z. Nie, P. Zuo, G. Li, T. Liu, J. Xiao, Y. Cheng, C. Wang, J.-G. Zhang, J. Liu, Nano Lett. 14 (2014) 255–260.
[9] L.R. Parent, Y. Cheng, P.V. Sushko, Y. Shao, J. Liu, C.-M. Wang, N.D. Browning, Nano Lett. 15 (2015) 1177–1182.
[10] F. Murgia, L. Stievano, L. Monconduit, R. Berthelot, J. Mater. Chem. A 3 (2015) 16478–16485.
[11] F. Murgia, E.T. Weldekidan, L. Stievano, L. Monconduit, R. Berthelot, Electrochem. Commun. 60 (2015) 56–59.
[12] N. Singh, T.S. Arthur, C. Ling, M. Matsui, F. Mizuno, Chem. Commun. 49 (2012) 149–151.
[13] K. Periyapperuma, T.T. Tran, M.I. Purcell, M.N. Obrovac, Electrochim. Acta 165 (2015) 162–165.
[14] F. Murgia, D. Laurencin, E.T. Weldekidan, L. Stievano, L. Monconduit, M.-L. Doublet, R. Berthelot, Electrochim. Acta 259 (2017) 276-283.
[15] L. Blondeau, E. Foy, H. Khodja, M. Gauthier, J. Phys. Chem. C 123 (2018) 1120-1126.
[16] A.P. Hammersley, J. Appl. Crystallogr. 49 (2016) 646–652.
[17] K.C. Hewitt, L.Y. Beaulieu, J.R. Dahn, J. Electrochem. Soc. 148 (2001) A402–A410.
[18] F. Murgia, L. Monconduit, L. Stievano, R. Berthelot, Electrochim. Acta 209 (2016) 730–736.
[19] B. Zhang, R. Dugas, G. Rousse, P. Rozier, A.M. Abakumov, J.-M. Tarascon, Nat. Commun. 7 (2016) 10308.
[20] C. Marino, N. Dupré, C. Villevieille, J. Power Sources 365 (2017) 339–347.
[21] B. Predel, in: O. Madelung (Ed.), Hg-Ho – -Zr, Springer Berlin Heidelberg, Berlin, Heidelberg, 1997, pp. 1–5.
[22] T. Heumann, B. Predel, Z. Fuer Met. 57 (1966) 50–55.
[23] C. Suryanarayana, Prog. Mater. Sci. 46 (2001) 1–184.
[24] C. Tyzack, G.V. Raynor, Acta Crystallogr. 7 (1954) 505–510.

[25] P. Bhattacharya, K. Chattopadhyay, Int. J. Nanosci. 04 (2005) 909–920.
[26] M. Gauthier, D. Mazouzi, D. Reyter, B. Lestriez, P. Moreau, D. Guyomard, L. Roué, Energy Environ. Sci. 6 (2013) 2145–2155.
[27] J. Saint, M. Morcrette, D. Larcher, L. Laffont, S. Beattie, J.-P. Pérès, D. Talaga, M. Couzi, J.-M. Tarascon, Adv. Funct. Mater. 17 (2007) 1765–1774.
[28] B.C. Gerstein, F.J. Jelinek, M. Habenschuss, W.D. Shickell, J.R. Mullaly, P.L. Chung, J. Chem. Phys. 47 (1967) 2109–2115.
[29] A. Jain, S.P. Ong, G. Hautier, W. Chen, W.D. Richards, S. Dacek, S. Cholia, D. Gunter, D. Skinner, G. Ceder, K.A. Persson, APL Mater. 1 (2013) 011002.
[30] A. Jain, G. Hautier, S.P. Ong, C.J. Moore, C.C. Fischer, K.A. Persson, G. Ceder, Phys. Rev. B 84 (2011) 045115.
[31] T.F. Fässler, C. Kronseder, Zeitschrift für Kristallographie - New Crystal Structures, 214 (1999) 438.
[32] N. Ino, M. Hirabayashi, S. Ogawa, Trans. Jpn. Inst. Metals, 6 (1965) 172-178
[33] Y. Cheng, Y. Shao, L. R. Parent, M. L. Sushko, G. Li, P. V. Sushko, N. D. Browning, C. Wang, J. Liu, Adv. Mater. 27 (2015) 6598-6605.
[34] P. Limthongkul, Y.-I. Jang, N.J. Dudney, Y.-M. Chiang, Acta Mater. 51 (2003) 1103–1113.

Graphical Abstract

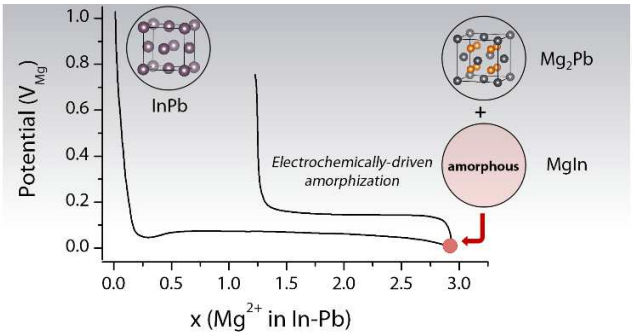

A In-Pb solid solution is investigated as negative electrode for Mg-ion battery and shows reversible alloying with upon magnesiation the formation of crystalline Mg_2Pb and an electrochemically-driven amorphization of MgIn.